A complete implementation of list-mode reconstruction for PET

ZHANG Bin[1] SHAN Baoci[2] YUN Mingkai[2] ZHAO Shujun[1,*]

[1] *Physical Engineering College, Zhengzhou University, Zhengzhou 450001, China*

[2] *Institute of High Energy Physics, Chinese Academy of Sciences, Beijing 100049, China*

Abstract Tomography reconstruction algorithm is one of the key components of positron emission tomography (PET) scanners, most PET scanners use statistical iterative reconstruction algorithms from data in sinograms currently. However tomography reconstruction using list-mode data has many unique advantages, in recent years great attention has been paid to it, being in the process of rapid development and improvement. In this paper, using experimental data of small animal PET scanner Eplus-166, exploiting ordinary subsetized list-mode EM (S-LMEM) algorithm and orthogonal distance-based ray-tracer (OD-RT), we eventually achieve list-mode tomography reconstruction. System response matrix (SRM), which establishes mapping relationship between the image and the projection space, is one key problem in iterative reconstruction algorithm. OD-RT is based on an optimization Siddon's algorithm to calculate the SRM, generating line-of-response (LOR) which is approximately Gaussian-shaped, achieving better modeling of detector response function (DRF). The results demonstrate that image resolution recovery achieves the inherent properties of the scanner and that on-the-fly ray-tracer for real-time calculation of system response matrix is feasible for dynamic reconstruction. Meanwhile, the optimal parameters for calculating SRM are found by experiments.

Key words Tomography reconstruction in PET, List-mode, Ray tracing, System response matrix

1 Introduction

Positron emission tomography (PET) is a powerful non-invasive tool to provide quantitative information of dynamic physiological and biochemical processes *in vivo*. A PET scanner consists of detector rings.

Without changing the physiological conditions of a subject, radioactive tracer is injected into the subject, involved in its metabolism. When the tracer decays, it emits a positron, which travels a short distance before annihilating with an electron, generating a pair of 511-keV γ photons travelling in nearly opposite directions. Using coincidence detection technique, the two photons form a coincidence event. A line connecting two relevant detectors is defined as a line-of-response (LOR), along which the annihilation takes place. Each LOR is characterized by a direction and the distance from the centre of gantry. Each coincidence event is assigned to a LOR. The number of coincidence events along a LOR is proportional to integral tracer concentration along the line. Each coincidence event can be recorded in a list-mode file or be accumulated into a sinogram. In the list-mode, the coincidence events are stored one by one in the form of a list, preserving all of the measured attributes of the detected photon pairs. Actually, sinogram is a matrix coming from rebinning and histo-gramming list-mode data. In the sinogram, the value in each pixel represents the number of coincidence events between the detectors associated with the LOR. After acquiring and correcting data, tomography reconstruction is conducted, generating time series images of tracer concentration distribution, and observing the metabolism *in vivo*.

2D and 3D or 4D images reconstructed by PET can reflect anatomical structure of tissues and organs, represent physiological and biochemical parameters and functional status of region of interest in animal body, as well as implement quantitative detection of physiological processes at molecular level, being the

* Corresponding author. *E-mail address*: zhaosj@zzu.edu.cn

Received date: 2012-02-22

most sensitive of all imaging modalities. PET has become an important tool in clinical medicine, especially in early diagnosis of cancer, brain function imaging and heart disease, and the basic equipment in many areas, such as cognitive neuroscience, molecular imaging, biomedical engineering, pharma-cokinetics, pharmacology and traditional Chinese medicine[1–3].

Tomography reconstruction algorithm is the key component of a PET system, for its performance and imaging quality. At present, most reconstruction algorithms use sinogram data, but list-mode data are of many advantages.

First, the preserved measurement information in list-mode data is maximized. In order to reduce demand of data storage, radial and axial data are often compressed in sinogram, and compression results in negative impact on image reconstruction quality[4,5]. Also, the number of bits per attribute is limited. Other ways to reduce demand of data storage are often adopted, i.e., mapping a large set of measured data attributes to a small set of estimate values. This may cause information loss, while list-mode data include energy, position, time of flight (TOF) etc, thus keeping the full spatial and temporal information. Therefore, with list-mode data, accurate image reconstruction and data post-processing can be implemented, and no additional time and storage cost is required. It is well known that TOF information can greatly improve image reconstruction quality[6,7] because it reduces the statistical noise and improve signal-to-noise ratio. However, it is very difficult to use TOF information in reconstruction algorithm based on sinograms.

Next, list-mode data provide a tremendous savings to storage requirements in dynamic reconstruction and condition of low statistical counts. In modern PET scanners, a rapid increase in the individual crystals is always accompanied with a sharp increase of the LORs. However, due to the count -limited nature of PET imaging, most of bins in sinogram actually may not measure any counts[4,5,8]. Especially, the period for dynamic reconstruction is usually short, resulting in small coincidence events in each frame. In sinogram, a LOR always takes up a storage unit, no matter whether there are coincidence events in the LOR. List-mode data can ignore the uncounted LORs, eliminating the storage of empty sinogram bins, leading to high efficiency of data storage[4,8]. For instance, high-resolution research tomograph (HRRT) adopts double-layer LSO/LYSO block which contains depth of interaction information. HRRT consists of 119 808 crystal strips, and has about 4.5 billion LORs at 3D data acquisition mode. For sinogram mode, if LORs are not compressed, each frame of dynamic reconstruction contains 10816 sinograms, about 8×10^8 bins, 1.6 GB of data. A ^{11}C dynamic study will produce 29 GB siongram data, but in fact, only about 5–6 GB list-mode data is collected[4,9]. Therefore, list-mode data can reduce the burden on computer systems and increases speed of image reconstruction by reducing the amount of disk reads, being particularly favorable for dynamic imaging and imaging in conditions of low statistical counts[9, 10]

Finally, list-mode reconstruction is easy to implement movement correction. Only accurate and feasible movement correction can lead to high-resolution clinical image. List-mode data may include information from respiratory gating and electrocardiographic gating, therefore movement correction is easy to implement in list-mode reconstruction.

In recent years, the list-mode reconstruction algorithm has attracted great attention due to its rapid development and improvement[4, 11–13].

2 List -mode reconstruction algorithm

List-mode reconstruction algorithm mainly includes: list-mode expectation maximization algorithm[13,14], ordinary subsetized list-mode EM algorithm, convergent subsetized list-mode EM algorithm (CS-LMEM), hybrid S/CS list-mode EM algorithm, the random subtraction list-mode EM algorithm including an image non-negativity constraint[4,5], accelerated list-mode EM algorithm by subsets in combination with a relaxation parameter[15], one-pass list-mode expectation maximization (OPL-EM)[10].

All these algorithms are based on statistical iterative method with different characteristics. S-LMEM algorithm derives from ordered subsets expectation maximization (OSEM) algorithm. It is not a convergent algorithm, and will produce limit cycles, resulting in alternating oscillations in image quality parameters. CS-LMEM is an additive algorithm retaining the previous image contribution for every subset. So it has properties of convergent resolution and contrast. Comparison CS-LMEM with S-LMEM shows that S- LMEM can produce higher quality image in the iterative process of the former subsets. Hybrid S/CS list-mode EM algorithm uses S-LMEM for the entire or part of the first iteration, then switches to CS-LMEM in the rest of the calculation to eliminate the limit cycles behavior. This algorithm combines the advantages of the two methods and can reach a higher image quality in a lower number of iterations, maintaining a convergent behavior. In the case of low statistical counts, accelerated list-mode EM algorithm and OPL-EM only need one or two iterations to achieve very good image quality, particularly being suitable for real-time image reconstruction[4,9–16].

In practice, with the consideration to PET scanner Eplus-166 characteristics, S-LMEM algorithm is mainly adopted as follows.

$$\lambda_j^{k,l} = \frac{\lambda_j^{k,l-1}}{s_j} \sum_{n=1}^{N} a_{ij} \frac{1}{q_i} \tag{1}$$

$$s_j = \sum_{i=1}^{I} a_{ij} \tag{2}$$

$$q_i = \sum_{j'=1}^{M} a_{ij'} \lambda_{j'}^{k,l-1} \tag{3}$$

where, $\lambda_j^{k,l}$ is the estimated value of voxel j after l^{th} (l=1,…, L) sub-iteration in k^{th}(k=1,…, K) iteration; a_{ij} is the probability of an emission from voxel j (j = 1,..., J) being detected along LOR i (i=1,..., I); I is the total number of LORs; J is the total number of image voxels; s_j is the sensitivity correction factor, i.e., the probability of any emission from voxel j being detected anywhere, representing the sensitivity of any point in system field of view; N is the number of the detected coincidence events in a subset l, and q_i is the expected counts in LOR i at present image intensity, also known as forward- projection.

S-LMEM algorithm comes from OSEM. In S-LMEM algorithm, list-mode data is subdivided into a sequence of subsets, each subset takes a fraction of the total duration of the data. Each of them can be deemed as a lower-statistics scan. This subdividing way naturally meets the requirement that maximize difference among subsets in OSEM. S-LMEM algorithm does no converge at fixed point, because each subset is an independent Poisson process, each owns different maximum likelihood estimation value.

3 System response matrix calculations

A key problem in statistical reconstruction algorithm is the RSM, which establishes mapping relationship between the image and the projection space, as Eq.(4).

$$p_i = \sum_{j=1}^{J} a_{ij} \lambda_j + e_i \tag{4}$$

where, p_i is the measured projection along LOR i; a_{ij} is the probability that a positron from voxel j results in the detection of a coincidence event along i^{th} LOR; λ_j represents the original radioactivity distribution in voxel j; and e_i is the statistical noise in the projection.

SRM can incorporate various physical effects, such as the particular system geometry, random coincidences, scatter, the attenuation in the subject, positron range, non-collinearity, crystal penetration, inter-crystal scatter and so on. In any case, the main factor of the SRM is the geometrical component[20]. In particular, due to the intrinsically LOR-based nature of list-mode reconstruction, which must be performed event by event, computing the elements of the SRM on the fly is well suited for list-mode reconstruction. In order to improve computational efficiency, only geometry effect is considered.

Geometric effect calculation is implemented by analytical methods, including Siddon's algorithm, bilinear interpolation, trilinear interpolation and Wu anti-aliased algorithm. Siddon's algorithm has higher efficiency but less poor accuracy. The other three algorithms can lead to better images but more computational cost[16–20].

In practice, the OD-RT method, which mainly accounts for geometrical effect, is implemented [20],

$$a_{ij}=1-(d_{ij}/\delta) \tag{5}$$

where, d_{ij} is orthogonal distance between pixel centre and LOR; and δ is a parameter relating to full width at half maximum (FWHM) of point spread function (PSF) of PET detectors, to determine the size of the LORs.

LORs generated with Siddon's algorithm are relatively thin and consequently cannot well match with detector of certain width. Based on an optimization Siddon's algorithm, the generated LORs by OD-RT are approximately Gaussian-shaped, and can accurately model DRF (Fig.1). First, the minimum threshold of a_{ij} is set to control the number of pixels relating to a LOR and increase efficiency of computing the elements of SRM. Then optimization Siddon's algorithm is used to find those pixels crossed by the LOR and their adjacent pixels. The orthogonal distances between pixels and LORs and weights of pixels are computed. If the weights obtained are greater than the threshold value, the pixels are retained. A compromise must be reached between the cost of computation and image quality, so setting the minimum threshold of a_{ij} properly is crucial.

Two sets of equally spaced parallel planes are perpendicular to an x- and y-axis respectively, to determine the pixel space. The number of x- and y-planes equals N_x and N_y, the distance between planes are denoted by d_x and d_y, respectively. Shaded areas represent an approximately Gaussian-shaped LOR generated by OD-RT method. The greyscale of pixel is proportional to the detection probability of positron emission in pixel for a given LOR.

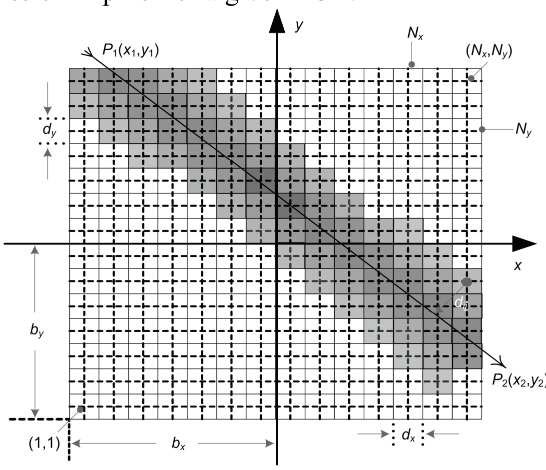

Fig.1 Schematic of OD-RT method.

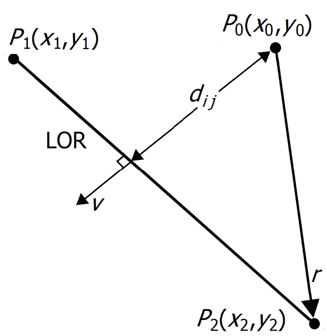

Fig.2 Schematic of calculating the distance from geometric centre of pixel to LOR.

As shown in Fig.2, let $P_0(x_0, y_0)$ be the geometric centre of pixel, $P_1(x_1, y_1)$ and $P_2(x_2, y_2)$ be endpoints of LOR, $\boldsymbol{v}$ be a unit vector perpendicular to the LOR, and $\boldsymbol{r}$ be a vector from $P_0(x_0, y_0)$ to P_1 or P_2 the distance d_{ij} from geometric centre of pixel to LOR is given by projecting $\boldsymbol{r}$ onto $\boldsymbol{v}$ in Eq.(6).

$$d_{ij} = |\boldsymbol{v} \cdot \boldsymbol{r}| = \frac{|(x_2 - x_1)(y_1 - y_0) - (x_1 - x_0)(y_2 - y_1)|}{\sqrt{(x_2 - x_1)^2 + (y_2 - y_1)^2}} \tag{6}$$

4 Experiment equipment and materials

Eplus-166, the first small animal PET with independent intellectual property right in China, is developed and fabricated by Institute of High Energy Physics, Chinese Academy of Sciences. This scanner consists of 16 modules in a regular hexadecagon. Each module is made up of two blocks in axial arrangement and each block contains 16×16 LYSO crystals. Each crystal is of 1.9 mm×1.9 mm×10 mm in size. In order to improve the light collection efficiency, the gap between the crystals is filled with reflective material, resulting in detector size of 2.0 mm×2.0 mm along the axial and transaxial direction. The entire Eplus-166 forms 32 detector rings in axial length of 64 mm. Fig.3 shows its structure and Table 1 lists the parameters[21].

Table 1 Eplus-166 system parameters.

Ring diameter / mm	166
Detector ring	32
Crystals /ring	256
Crystal size / mm	1.9 ×1.9×10
Transaxial field of view / mm	110
Axial field of view / mm	64
Maximum ring difference	31

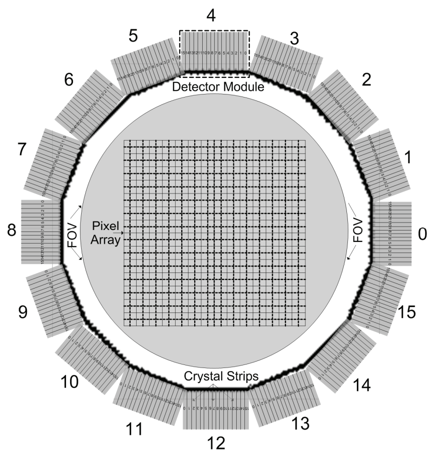

Fig.3 Schematic for Eplus-166 structure.

A self-made Derenzo phantom containing capillaries is used for algorithm verification.. Their diameters in six sectors are 1.4, 1.6, 1.9, 2.2, 2.5 and 3.0 mm, respectively. The distance between capillaries centres is twice of the diameter. The phantom is filled with ^{18}F-FDG and scanned on the Eplus-166 system. After acquired data are normalized, the scatter and attenuation, list-mode iterative reconstruction is executed.

5 Results and Analysis

Only 2D tomography reconstruction for algorithm verification is implemented. S-MLEM algorithm is exploited to achieve image reconstruction, with orthogonal distance-based ray-tracer adopted to calculate SRM on the fly. The variable δ in Eq.(5) is set as 3.0, 2.5, 2.0, 1.8, 1.5, 1.2, 1, 0.8, and 0.5, but only results of δ=1.5, 1.2, 1, 0.8 and 0.5 are indicated in Figs.(4) and (5).

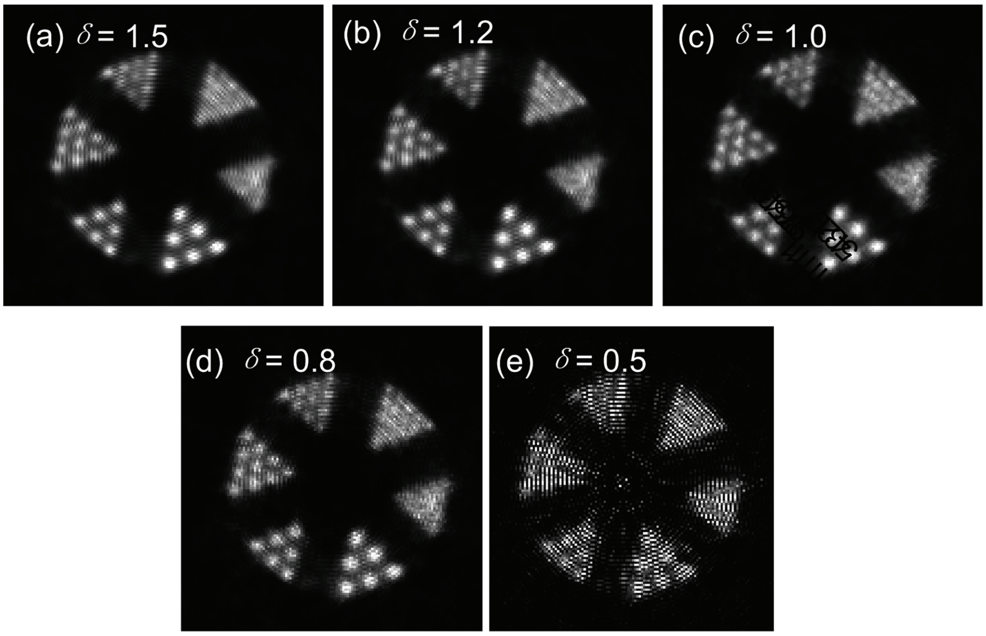

Fig.4 Comparison of image reconstruction results using S-MLEM.

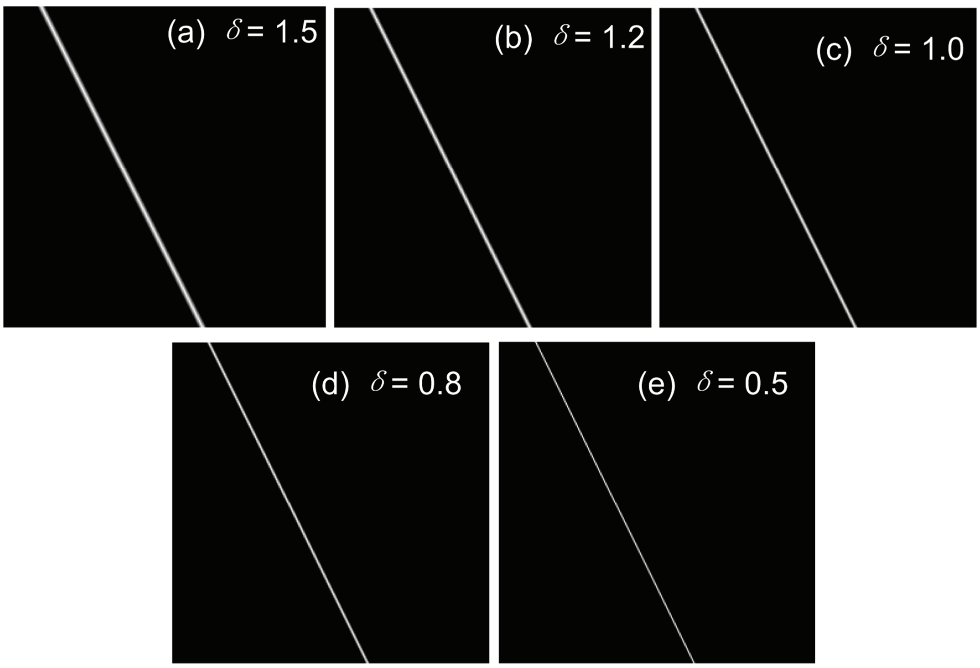

Fig.5 Shapes of LOR generated by OD-RT.

When using 1 615 130 coincidence events within 47th direct slice in experimental data, these events are divided into 32 subsets, there are about 50 000 events in each subset. Reconstruction results and the corresponding LORs are shown in Figs.(4) and (5). From reconstruction results, the calculating precision of SRM can play a crucial role in resolution recovery. When using orthogonal distance-based ray-tracer to calculate SRM, it is a key to select the proper δ value. FWHM of point spread function of centre field-of-view in Eplus-166 is about 1.67 mm[21]. At δ=1, the effect is the best. The 1.9- mm and some 1.6-mm hot spots can clearly be distinguished.

In small animal PET scanners, the size of the LORs determines their main properties, such as maximum resolution and the signal to noise ratio. The physical effects during acquisition of PET data cause the LOR to have a certain width. Wide LORs will yield low noise levels with poor resolution in PET reconstruction. While thin LORs try to recover higher frequencies, resulting in an increase of the noise level. The LOR in Fig.5 is wide with δ=1.5 while the LOR is thin with δ = 0.5.

The OD-RT method already incorporates a built-in PSF model based on a linear kernel[20]. In case of an appropriate δ value, the linear kernel approximates Gaussian blur function for PET detector and achieves better modeling DRF.

Figure 4 shows that the image of 1.6 mm hot spot area becomes blur with δ=1.5(the image becomes more blur with δ=1.8, 2.0, 2.5, 3.0), better image quality is achieved with δ=1.0 (similar effects can be obtained with δ=1.2, 0.8), and aliasing artifacts appear obviously with δ= 0.5. Therefore, when δ value is about half of the 1.9-mm crystal width, image quality is good.

6 Conclusions

In this paper, list-mode data and on-the-fly ray-tracer for real-time calculation of system response matrix is feasible for dynamic reconstruction. It would help to further study dynamic reconstruction, reconstruction in conditions of low statistical counts and TOF reconstruction.

List-mode reconstruction is performed event by event and is a computationally intensive task. Program implementation should use parallel programming techniques, taking full advantage of the multi-threading and multi-core computer systems to speed up programs. The message passing interface is adopted.

Along with computer software and hardware technology development, fully 3D tomography reconstruction has become key and hot spot in PET after solving huge amount of calculation and storage problems gradually, to further achieve the reasonable and effective data.

Acknowledgement

I thank all the members of the Nuclear Medicine Imaging Group at the Key Laboratory of Nuclear Analysis Techniques of China Institute of High Energy Physics for their help. This work was supported by grants from the National Natural Science Foundation of China (81171410).

References

1 Jin Y J, Ma T Y. Nucl Med Instrum Meth. 1rd ed. Harbin: Harbin Engineering University Press, 2009, 184–228. (in Chinese)
2 Herzog H. Radiat Phys Chem, 2007, **76:** 337–342.
3 Tian J H. People's Military Surgeon, 2004, **47:** 229– 232.
4 Rahmim A, Lenox M, Reader A J, *et al.* *Ph*ys Med Biol, 2004, **49:** 4239–**42**58.
5 Rahmim A, Cheng J C, Blinder S, *et al. Phys* Med Biol, 2005, **50: 4887**–4912
6 Conti M. Phys Med, 2009, **25:** 1–11.
7 Groiselle C J, Glick S J. M2-305: 3D PET List-mode iterative reconstruction using time-of-flight information
8 Wienhard K, Schmand M, Casey M E, *et al.* IEEE Trans Nucl Sci 2002, **49:** 104–110.
9 Walledge R J, Reader A J, Aboagye E O, *et al.* M11-100: 4D PET with the quad-HIDAC: Development of dynamic list-mode EM image reconstruction. Nuclear science symposium medical imaging conference, Norfolk, Virginia USA, November 2002, 1716–1720.
10 Reader A J, Ally S, Bakatselos F, *et al*. IEEE Trans Nucl Sci, 2002, **49:** 693–699.
11 Shu J, Zhao S J, Shan B C.Chin J Med Imaging Technol,

2007, **23:** 937–939.

12 Musmann P, Schramm N U, Pietrzyk U, *et al*. M03-274: List-mode image reconstruction for the high resolution clear PETTM neuro system. Nuclear science symposium medical imaging conference, Puerto Rico, October 2005, 1770–1773.

13 Barrett H H, White T, Parra L C. J Opt Soc Am A, 1997, **14:** 2914–2923.

14 Parra L, Barrett H H. IEEE Trans Med Imaging, 1998, **17:** 228–235.

15 Reader A J, Manavaki R, Zhao S, *et al*. IEEE Trans Nucl Sci, 2002, **49:** 42–49.

16 Brinks R, Schretter C, Meyer C. M11-389: Comparison of maximum-likelihood list-mode reconstruction algorithms in PET. Nuclear science symposium medical imaging conference, San Diego CA, USA, October 2006, 2801–2803.

17 Schretter C. IEEE Trans Med Imaging, 2009, **18:** 117–124.

18 Zhao H X, Reader A J. M10-104: Fast projection algorithm for voxel arrays with object dependent boundaries, Nuclear science symposium medical imaging conference, Norfolk, Virginia USA, November 2002, 1490–1494.

19 Schretter C. Med Phys, 2006, **33:** 4744–4748.

20 Aguiar P, Rafecas M, Ortuño J E, *et al*. Med Phys, 2010, **37:** 5691–5702.

21 Yun M K. Fully 3D iteration image reconstruction for positron emission tomography, PhD. Beijing: Institute of High Energy Physics, Chinese Academy of Sciences, 2009, 63–113.